Journal of Nonlinear Modeling and Analysis
Volume 4, Number 2, June 2022, 371–391
http://jnma.ca; http://jnma.ijournal.cn
DOI:10.12150/jnma.2022.371

Noise-induced Transitions for an SIV Epidemic Model with Medical-resource Constraints*

Ran Yu[1], Anji Yang[1] and Sanling Yuan[1,†]

Abstract We consider a stochastically forced epidemic model with medical-resource constraints. In the deterministic case, the model can exhibit two type bistability phenomena, i.e., bistability between an endemic equilibrium or an interior limit cycle and the disease-free equilibrium, which means that whether the disease can persist in the population is sensitive to the initial values of the model. In the stochastic case, the phenomena of noise-induced state transitions between two stochastic attractors occur. Namely, under the random disturbances, the stochastic trajectory near the endemic equilibrium or the interior limit cycle will approach to the disease-free equilibrium. Besides, based on the stochastic sensitivity function method, we analyze the dispersion of random states in stochastic attractors and construct the confidence domains (confidence ellipse or confidence band) to estimate the threshold value of the intensity for noise caused transition from the endemic to disease eradication.

Keywords Epidemic model, Medical-resource constraints, Noise-induced transitions, Stochastic sensitivity, Confidence domain.

MSC(2010) 34K50, 60H10, 93E03.

1. Introduction

Mathematical models play an indispensable role in epidemiological research. For instance, Sun et al., [16] analyzed an SIS model incorporating the effects of awareness spreading on epidemic. In the past few decades, scholars have proposed various epidemic models to explore the complex spreading process and test the effectiveness of disease control after the introduction of interventions [7–9, 20, 26]. In the classical epidemic models, it is usually assumed that the medical resources such as drugs, vaccines and hospital beds are very sufficient for the infectious disease. However, the reality is that medical resources are usually limited. In order to investigate the dynamics of disease transmission under the absence of medical resources, some epidemic models with medical-resource constraints have been proposed. For example, Zhang et al., [25] introduced a saturated treatment function in an SIR model to describe the limited medical resources. Zhu et al., [14] defined a more complex saturated function to characterize the impact of hospital beds on disease control, and their results show that the model can experience a sequence of bifurcations

†the corresponding author.
Email address: Sanling@usst.edu.cn (S. Yuan), yuran_math@163.com (R. Yu), Anji_Yang_715@163.com (A. Yang)
[1]College of Science, University of Shanghai for Science and Technology, Shanghai 200093, China
*The authors were supported by National Natural Science Foundation of China (No. 12071293).

including Hopf bifurcation, saddle-node bifurcation, backward bifurcation. Wang et al., [19] first adopt a piecewise-defined treatment function to simulate a limited capacity for treatment. Then, they further modified the treatment function into the following form [18]

$$T(I) = \begin{cases} rI, & 0 \le I \le I_0, \\ rI_0, & I > I_0, \end{cases}$$

which means that the treatment rate is proportional to the case number before the capacity of treatment is reached, then take its maximum value rI_0. Recently, using a similar idea as described in Ref. [18], Wang and Xiao et al., [17] has put forward an SIV epidemic model with a non-smooth but continuous function that depicts vaccination strategies. Their analysis suggested that this model undergoes the following three types of bistability: between two internal equilibrium, between one disease-free equilibrium and one endemic equilibrium, or between one disease-free equilibrium and one limit cycle.

Although the above deterministic models based on constant environmental settings can always capture some hallmarks of disease transmission, unexpected stochastic factors such as resource availability, humidity and temperature, play an indispensable role in the spread of disease. For instance, Mecenas et al., [11] found that the replicability and the transmission capacity of the COVID-19 virus goes hand in hand with different weather conditions such as temperature and relative humidity. In addition, the unpredictability of human-to-human contact is also one of the stochastic drivers in the spread of epidemics when populations are small [15]. Therefore, it is necessary to probe the influence of noisy environmental fluctuations on the disease transmission. To this end, Lan et al., [10] put forward a SIRS epidemic model disturbed by a noisy environment and explored the influence of hospital resources on the final scale of infection. Cai et al., [5] investigated a SIRS model subject to stochastic noise and revealed that environmental fluctuations can restrain disease outbreaks.

For highly nonlinear models, the stochasticity of the environment may push the system back and forth between two metastable states. In recent years, the work related to noise-induced transitions has been extensively considered by mathematicians, ecologists and physicists in various fields. For example, in the field of meteorology, Yang et al., [23] used the maximum possible trajectory to simulate the sudden jump behavior of a stochastic thermohaline circulation model between initial and final states. In the field of biology, Chen et al., [6] multiplicatively introduced non-Gaussian noise into a genetic regulatory model and implemented high-order perturbation expansion technique to calculate the average transition time of protein concentration from low to high. In the field of ecosystem, Scheffer et al., [13] proposed various warning signals for the bifurcation-induced critical transitions to avoid the undesirable state of ecosystem. Xu [21] probed the dynamics mechanisms behind the population size oscillatory transition in a predator-prey model.

For the noise-induced state transition phenomenon, a question worth exploring is how large is the critical noise intensity that can cause a system state transition? The stochastic sensitivity function (SSF) method proposed by Bashkirtseva et al., [1, 12] can effectively answer this problem. This method employs confidence ellipse or confidence band to visualize the spatial arrangement of random states near the deterministic attractors such as the endemic equilibrium or the interior limit cycle. Therefore, we can regard the noise intensity when the confidence ellipse

or confidence band is tangent to the boundary of the domain of attraction as the critical noise intensity. Based on the SSF method, Yuan et al., [24] studied a stoichiometric producer-grazer model subject to the Gaussian white noise and obtained the critical noise intensity when the random trajectory transitions between a high biomass state and a low biomass state. Moreover, Yang et al., [22] applied this method to a stochastic non-smooth SIS epidemic model, and also gave the critical noise intensity when the final number of infected people switched between low and high.

This manuscript is organized as follows: In Section 2, we first summarize the key results of the deterministic model (2.1), which is the basis of subsequent analysis, and then introduce Gaussian white noise into the deterministic version to obtain its random counterpart. The surveys of noise-induced state shifts from an endemic equilibrium to a disease-free equilibrium by constructing the confidence ellipses will be presented in Section 3. In Section 4, we analyze the phenomenon of noise-induced state shifts from an internal limit cycle to a disease-free equilibrium by constructing the confidence band. Section 5 is the conclusion.

2. Mathematical model

2.1. Deterministic model

In this section, we consider the following SIV epidemic model with nonlinear incidence rate and medical-resource constraints:

$$\begin{aligned} \frac{dS}{dt} &= \Lambda - \beta SI^2 - mS - H(S), \\ \frac{dI}{dt} &= \beta SI^2 - mI - \epsilon I, \\ \frac{dV}{dt} &= H(s) - mV. \end{aligned} \tag{2.1}$$

Here, $S(t)$, $I(t)$ and $V(t)$ are the sizes of susceptible, infected and immune population at time t, respectively. All parameters of the model (2.1) are non-negative. Λ denotes the recruitment rate; β presents the transmission rate; m is the natural death rate; ϵ denotes the disease-induced death rate. In [17], the authors proposed the following function

$$H(S) = \begin{cases} rS, & S \le S_c, \\ rS_c, & S > S_c, \end{cases} \tag{2.2}$$

which defines a vaccination strategy as follows: when the size of the susceptible population is less than the threshold S_c, we take a vaccination rate that is directly proportional to the susceptible population size. Otherwise, the vaccination rate is a constant $k = rS_c$.

Since the dynamics of the first two equations are not affected by the vaccination compartment, we analyze the following equations:

$$\begin{aligned} \frac{dS}{dt} &= \Lambda - \beta SI^2 - mS - H(S), \\ \frac{dI}{dt} &= \beta SI^2 - mI - \epsilon I. \end{aligned} \tag{2.3}$$

We set $N = S + I + V$, and have

$$\frac{dN}{dt} = \Lambda - mN - \epsilon I.$$

Denote

$$\Omega = \left\{ (S, I) \in R_+^2 : 0 < S + I < \frac{\Lambda}{m} \right\}.$$

It is easy to verify that Ω is a positively invariant set for system (2.3). Then, in [17], a complete qualitative analysis of global dynamics for model (2.3) is presented by Wang et al. Here, we just demonstrate the following essential results.

Lemma 2.1. *(Theorem 5.6 of [17]) Assume that $\epsilon > m + 2r$, (i) if $\max\{M_4, \overline{\eta}_2\} < \beta < \min\{M_2, \overline{\eta}_1\}$ or $\beta > M_2$, then model (2.3) has two internal equilibrium E_*, E_1 and one boundary equilibrium E_0, where E_* and E_0 are stable and E_1 is a saddle. All solutions above the stable manifold of E_1 approach the endemic equilibrium E_*, and the solutions below the stable manifold of E_1 will tend to E_0.*
(ii) If $\max\{M_4, \overline{\eta}_1\} < \beta < M_2$ or $M_4 < \beta < \min\{M_2, \overline{\eta}_2\}$ or $\beta < M_4$, then model (2.3) has a stable boundary equilibrium E_0. Variation of system parameters leads to a Hopf bifurcation, where internal equilibrium point E_* loses its stability, and the limit cycle Γ bifurcates from this equilibrium. The stable manifold of E_1, the boundary of the basin of the attraction, divides the first quadrant into two parts. All solutions above the boundary approach Γ. Otherwise, they tend to E_0, where

$$M_1 = \frac{2(m+\epsilon)^2(m+\epsilon+r)}{\Lambda^2}, \quad M_2 = \frac{(m+\epsilon)^2(m+\epsilon+r)^2}{\epsilon\Lambda},$$

$$M_3 = \frac{2(m+\epsilon)^3}{\Lambda^2}, \quad M_4 = \frac{(m+\epsilon)^4}{\Lambda^2(\epsilon - r)}.$$

and

$$\eta_1 = (m+\epsilon)^2[4m + 4\epsilon + r + \sqrt{12\epsilon^2 + 8\epsilon m + r^2 + 4m^2 - 8\epsilon r}],$$

$$\eta_2 = (m+\epsilon)^2[4m + 4\epsilon + r - \sqrt{12\epsilon^2 + 8\epsilon m + r^2 + 4m^2 - 8\epsilon r}],$$

$$\overline{\eta}_1 = \frac{\eta_1^2}{2\Lambda^2(m+\epsilon)^2[2m + 4\epsilon - r + \sqrt{12\epsilon^2 + 8\epsilon m + r^2 + 4m^2 - 8\epsilon r}]},$$

$$\overline{\eta}_2 = \frac{\eta_2^2}{2\Lambda^2(m+\epsilon)^2[2m + 4\epsilon - r - \sqrt{12\epsilon^2 + 8\epsilon m + r^2 + 4m^2 - 8\epsilon r}]}.$$

We take the same parameters in [17]:

$$\Lambda = 3, \quad m = 0.2, \quad r = 0.25, \quad \epsilon = 0.8, \quad S_c = 2.8128,$$

and vary the infectious rate $\beta \in [0.231, 0.239]$. Three different regimes of dynamics for model (2.3) are showed in Figure 1.

When $\beta > \beta^* = 0.237$, the endemic equilibrium E_* is stable. As the parameter β decreases gradually, the endemic equilibrium E_* loses stability and a limit cycle is formed around it. The parameter value β^* is the Hopf bifurcation point. For $\beta = 0.239 > \beta^*$, the attraction domains of the disease-free equilibrium E_0 and the endemic equilibrium E_* are clearly separated by the stable manifold of E_1 (see Figure 1(c)). All solutions above the boundary approach the endemic equilibrium E_*, and the solutions below the boundary will tend to E_0. This indicates that

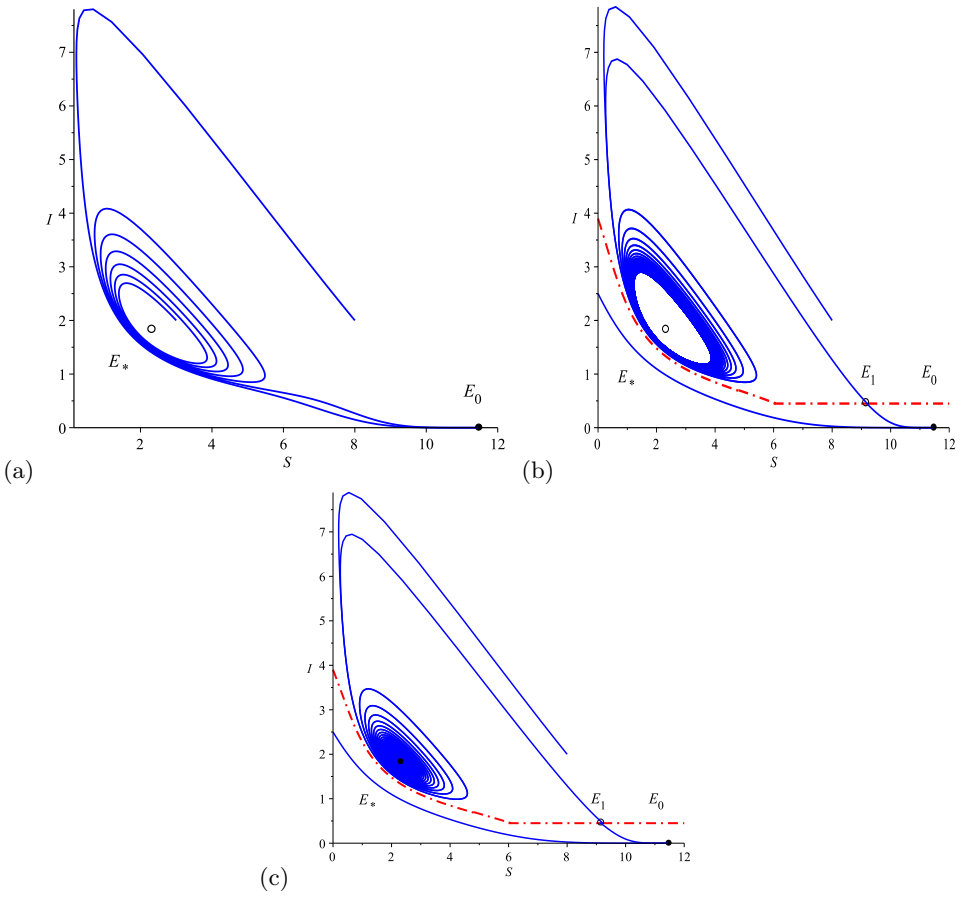

Figure 1. Phase plane of the deterministic model (2.3) for (a) $\beta = 0.231$; (b) $\beta = 0.235$; (c) $\beta = 0.239$

the initial number of susceptible and infected individuals determine the final state of disease. For $\beta = 0.235 < \beta^*$, the stable manifold of E_1 detach domains of the attraction of disease-free equilibrium E_0 and the stable limit cycle Γ (see Figure 1(b)). The solutions starting from above the boundary will ultimately approach the limit cycle. At this point, the number of infected individuals changes periodically and the disease can not be eliminated. As the parameter β continues to decrease, the limit cycle gradually expands and eventually disappears (see Figure 2). For $\beta = 0.231 < \beta_* = 0.233$, E_* is unstable, and the boundary between the two attraction basins (red dash-dotted) is broken. All the solutions of model (2.3) eventually approach the disease-free equilibrium E_0 (see Figure 1(a)). So this suggests that the whole first quadrant coincides with the disease extinction region.

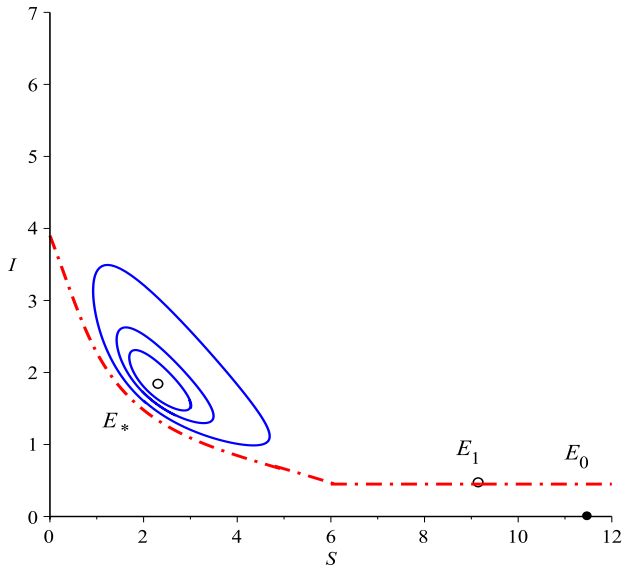

Figure 2. Separatrix (red dashed-dotted) and deterministic cycles (blue solid) for $\beta = 0.237$(small), $\beta = 0.235$(middle), $\beta = 0.233$(large)

The Hopf bifurcation diagram of model (2.3) is shown in Figure 3. Here, dashed line corresponds to the I-coordinate of the unstable endemic equilibrium E_* and the red star represents the bifurcation point β^*. Next, we describe the quantitative dynamical features of the deterministic model (2.3) for endemic equilibrium E_* by the largest Lyapunov exponent (LLE). LLE Λ is commonly used as a quantitative measure of the internal dynamics. When LLE is negative, the random trajectories of model (2.3) mostly converge. Otherwise, the divergence dominates in stochastic flow [2]. In Figure 4, as the parameter β changes from right to left, the sign of LLE becomes positive from negative at the bifurcation point β^*. This indicates that the stability of endemic equilibrium E_* has changed.

2.2. Stochastic model

Considering the presence of ambient noise, the parameters of model (2.3) are never constant but fluctuate around some certain values. Notice that the infectious rate

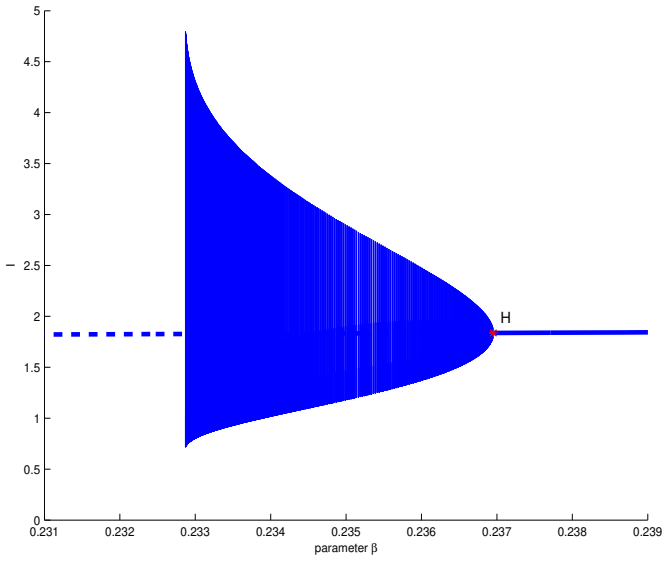

Figure 3. Hopf bifuraction diagram of model (2.3)

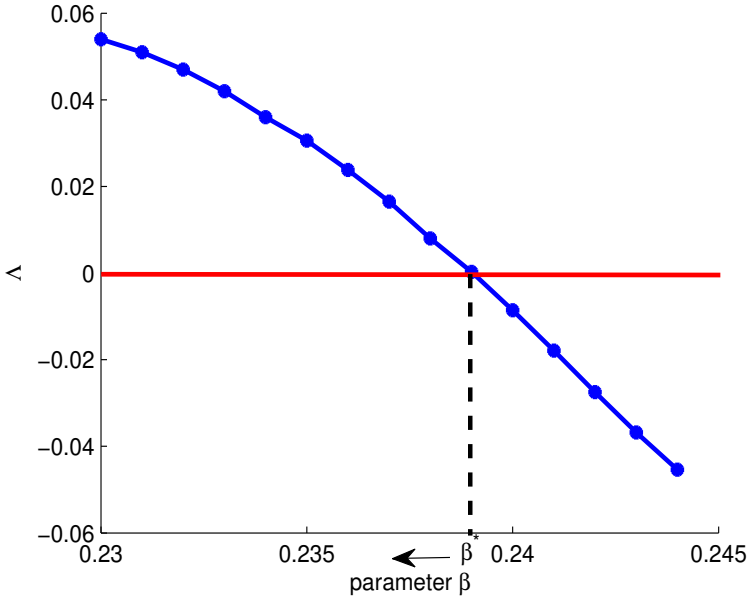

Figure 4. The largest Lyapunov exponents for endemic equilibrium E_*

β is one of the important parameters in the model and is significantly affected by environmental fluctuations. Thus, we introduce random factor into model (2.3) by disturbing valid contact coefficient β by $\beta+\sigma\dot{B}(t)$ and get the stochastic differential equations as follows:

$$\begin{aligned} dS &= [\Lambda - \beta SI^2 - mS - H(S)]dt - \sigma SI^2 dB, \\ dI &= [\beta SI^2 - mI - \epsilon I]dt + \sigma SI^2 dB, \end{aligned} \tag{2.4}$$

where $B(t)$ is a standard Brownian motion, σ denotes the noise intensities. We shall verify that stochastic model (2.4) has a global positive solution.

Lemma 2.2. *For any initial value $(S(0), I(0)) \in \Omega$, there is a unique solution $(S(t), I(t))$ of model (2.4) on $t > 0$, and the solution will remain in R^2_+ with probability 1.*

Proof. Let $(S(0), I(0)) \in \Omega$. Summing equations of system (2.4), we can obtain that

$$\frac{d(S(t)+I(t))}{dt} = \Lambda - mS - mI - \epsilon I - H(s) \leq \Lambda - (S+I)m.$$

Then, we have

$$\lim_{t\to\infty} sup(S(t)+I(t)) \leq \frac{\Lambda}{m}.$$

Namely, for any $s \in [0, t]$, we get

$$S(s), I(s) \in (0, \frac{\Lambda}{m}) \qquad a.s..$$

We assume that $S(0) > S_c$. Let us introduce the following stopping time sequence $\{\tau_i\}, i = 1, 2, \cdots$

$$\tau_1 = \inf\{t \geq 0, S(t) \leq S_c\}, \qquad \tau_2 = \inf\{t \geq \tau_1, S(t) > S_c\}$$

and

$$\tau_{2n+1} = \inf\{t \geq \tau_{2n}, S(t) \leq S_c\}, \qquad \tau_{2n+2} = \inf\{t \geq \tau_{2n+1}, S(t) > S_c\}$$

for $n = 1, 2, \cdots$. When $t \in [\tau_{2n}, \tau_{2n+1})$, model (2.4) becomes

$$\begin{aligned} \mathrm{d}S &= \left[\Lambda - \beta SI^2 - mS - rS_c\right] \mathrm{d}t - \sigma SI^2 \mathrm{d}B, \\ \mathrm{d}I &= \left[\beta SI^2 - mI - \epsilon I\right] \mathrm{d}t + \sigma SI^2 \mathrm{d}B, \end{aligned} \tag{2.5}$$

and when $t \in [\tau_{2n+1}, \tau_{2n+2})$, model (2.4) becomes

$$\begin{aligned} \mathrm{d}S &= \left[\Lambda - \beta SI^2 - mS - rS\right] \mathrm{d}t - \sigma SI^2 \mathrm{d}B, \\ \mathrm{d}I &= \left[\beta SI^2 - mI - \epsilon I\right] \mathrm{d}t + \sigma SI^2 \mathrm{d}B, \end{aligned} \tag{2.6}$$

where $n = 0, 1, 2, \cdots$ and $\tau_0 = 0$. For any initial value $(S(0), I(0)) \in \Re^2_+$, (2.5) and (2.6) both have a unique global positive solution, which implies model (2.4) has a unique local positive solution $(S(t), I(t))$ on $[0, \tau_e)$, where τ_e is the explosion time.

To show the solution is global, we only need to prove $\tau_e = \infty$ almost surely. Let $k_0 > 0$ be sufficiently large such that $S(0)$ and $I(0)$ both lie within the interval $\left[\frac{1}{k_0}, k_0\right]$. For all integer $k > k_0$, we define the stopping time

$$\tilde{\tau}_k = \inf\left\{t \in [0, \tau_e) : \min\{S(t), I(t)\} \leq \frac{1}{k} \text{ or } \max\{S(t), I(t)\} \geq k\right\}.$$

Clearly, $\tilde{\tau}_k$ is an increasing function as $k \to \infty$. Let $\tilde{\tau}_\infty = \lim_{k\to\infty} \tilde{\tau}_k$, whence $\tilde{\tau}_\infty \leq \tau_e$, *a.s.* If we can prove $\tilde{\tau}_\infty = \infty$, then $\tau_e = \infty$, and $(S(t), I(t)) \in \Re^2_+$ for all $t \geq 0$, *a.s.* Hence, we only need to show that $\tilde{\tau}_\infty = \infty$, *a.s.* We prove this by contradiction. If this assertion is false, then there exists a pair of constants $T > 0$ and $\varepsilon \in (0, 1)$ such that $P\{\tilde{\tau}_\infty \leq T\} > \varepsilon$. Hence, there exists $k_1 > k_0$ such that

$$P\{\tilde{\tau}_k \leq T\} \geq \varepsilon \tag{2.7}$$

for all $k \geq k_1$. Define a nonnegative $\mathcal{C}^2$-function $V : \Re^2_+ \to \Re_+$ by

$$V(S, I) = S - 1 - \ln S + I - 1 - \ln I.$$

Applying Itô's formula, we obtain respectively from (2.5) and (2.6) that for $t \in [\tau_{2n}, \tau_{2n+1})$,

$$\begin{aligned}
\mathrm{L}V(S, I) =& \left(1 - \frac{1}{S}\right)\left[\Lambda - \beta SI^2 - mS - H(S)\right] \\
&+ \left(1 - \frac{1}{I}\right)\left[\beta SI^2 - mI - \epsilon I\right] + \frac{1}{2}\sigma^2 I^4 + \frac{1}{2}\sigma^2 S^2 I^2 \\
\leq& \Lambda + 2m + \epsilon + \frac{1}{2}\sigma^2\left(\frac{\Lambda}{m}\right)^4 + \frac{1}{2}\sigma^2\left(\frac{\Lambda}{m}\right)^4 + \beta\left(\frac{\Lambda}{m}\right)^2 + \frac{H(S)}{S},
\end{aligned}$$

and that for $t \in [\tau_{2n+1}, \tau_{2n+2})$,

$$\begin{aligned}
\mathrm{L}V(S, I) =& \left(1 - \frac{1}{S}\right)\left[\Lambda - \beta SI^2 - mS - H(S)\right] \\
&+ \left(1 - \frac{1}{I}\right)\left[\beta SI^2 - mI - \epsilon I\right] + \frac{1}{2}\sigma^2 I^4 + \frac{1}{2}\sigma^2 S^2 I^2 \\
\leq& \Lambda + 2m + \epsilon + \frac{1}{2}\sigma^2\left(\frac{\Lambda}{m}\right)^4 + \frac{1}{2}\sigma^2\left(\frac{\Lambda}{m}\right)^4 + \beta\left(\frac{\Lambda}{m}\right)^2 + \frac{H(S)}{S}.
\end{aligned}$$

From (2.2). we know

$$\frac{H(S)}{S} = \begin{cases} r, & S \in [0, S_c), \\ (0, r], & S \in [S_c, +\infty). \end{cases}$$

Therefore, for $t \in [\tau_{2n}, \tau_{2n+1})$,

$$\mathrm{L}V(S, I) \leq \Lambda + 2m + \epsilon + \frac{1}{2}\sigma^2\left(\frac{\Lambda}{m}\right)^4 + \frac{1}{2}\sigma^2\left(\frac{\Lambda}{m}\right)^4 + \beta\left(\frac{\Lambda}{m}\right)^2 + r := M_1$$

and

$$\mathrm{d}V(S, I) \leq M_1 \mathrm{d}t - \sigma(1 - \frac{1}{S})SI^2 \mathrm{d}B + \sigma(1 - \frac{1}{I})SI^2 \mathrm{d}B, \tag{2.8}$$

and that for $t \in [\tau_{2n+1}, \tau_{2n+2})$,

$$\mathrm{L}V(S,I) \leq \Lambda + 2m + \epsilon + \frac{1}{2}\sigma^2\left(\frac{\Lambda}{m}\right)^4 + \frac{1}{2}\sigma^2\left(\frac{\Lambda}{m}\right)^4 + \beta\left(\frac{\Lambda}{m}\right)^2 + r := M_2$$

and

$$\mathrm{d}V(S,I) \leq M_2\mathrm{d}t - \sigma(1-\frac{1}{S})SI^2\mathrm{d}B + \sigma(1-\frac{1}{I})SI^2\mathrm{d}B \tag{2.9}$$

We assume that $(\tilde{\tau}_k \wedge T) \in [\tau_{2m}, \tau_{2m+1})$ for some $n = m$ (same logic follows when $(\tilde{\tau}_k \wedge T) \in [\tau_{2m+1}, \tau_{2m+2})$). This together with (2.8) and (2.9) yields

$$\begin{aligned}
&V(S(\tilde{\tau}_k \wedge T), I(\tilde{\tau}_k \wedge T))\\
\leq& V(S(0), I(0)) + \sum_{n=0}^{m-1}\left(\int_{\tau_{2n}}^{\tau_{2n+1}} M_1\mathrm{d}t - \int_{\tau_{2n}}^{\tau_{2n+1}} \sigma(1-\frac{1}{S})SI^2\mathrm{d}B + \int_{\tau_{2n}}^{\tau_{2n+1}} \sigma(1-\frac{1}{I})SI^2\mathrm{d}B\right)\\
&+ \sum_{n=0}^{m-1}\left(\int_{\tau_{2n+1}}^{\tau_{2n+2}} M_2\mathrm{d}t - \int_{\tau_{2n+1}}^{\tau_{2n+2}} \sigma(1-\frac{1}{S})SI^2\mathrm{d}B + \int_{\tau_{2n+1}}^{\tau_{2n+2}} \sigma(1-\frac{1}{I})SI^2\mathrm{d}B\right)\\
&+ \int_{\tau_{2m}}^{\tilde{\tau}_k\wedge T} M_1\mathrm{d}t - \int_{\tau_{2m}}^{\tilde{\tau}_k\wedge T} \sigma(1-\frac{1}{S})SI^2\mathrm{d}B + \int_{\tau_{2m}}^{\tilde{\tau}_k\wedge T} \sigma(1-\frac{1}{I})SI^2\mathrm{d}B.
\end{aligned}$$

Taking the expectations on both sides of the above inequality leads to

$$\mathrm{E}V(S(\tilde{\tau}_k \wedge T), I(\tilde{\tau}_k \wedge T)) \leq V(S(0), I(0)) + M\mathrm{E}(\tilde{\tau}_k \wedge T),$$

where $M = \max\{M_1, M_2\}$. Thus,

$$\mathrm{E}V(S(\tilde{\tau}_k \wedge T), I(\tilde{\tau}_k \wedge T)) \leq V(S(0), I(0)) + MT. \tag{2.10}$$

Let $\Omega_k = \{\omega \in \Omega : \tilde{\tau}_k = \tilde{\tau}_k(\omega) \leq T\}$ for $k \geq k_1$ and, by (2.6), $P\{\Omega_k\} \geq \varepsilon$. Note that for every $\omega \in \Omega_k$, we have either $S(\tilde{\tau}_k, \omega)$ or $I(\tilde{\tau}_k, \omega)$ equals either k or $\frac{1}{k}$. Hence, $V(S(\tilde{\tau}_k, \omega), I(\tilde{\tau}_k, \omega))$ is no less than either

$$k - 1 - \ln k \text{ or } \frac{1}{k} - 1 + \ln k,$$

Then, it follows from (2.10) that

$$\begin{aligned}
&V(S(0), I(0)) + MT\\
\geq&\mathrm{E}[I_{\Omega_k} V(S(\tilde{\tau}_k, \omega), I(\tilde{\tau}_k, \omega))]\\
\geq&\varepsilon\left[(k - 1 - \ln k) \wedge \left(\frac{1}{k} - 1 + \ln k\right)\right],
\end{aligned}$$

where I_{Ω_k} is the indicator function of Ω_k. Letting $k \to \infty$, we have

$$\infty > V(S(0), I(0)) + MT = \infty,$$

a contradiction. Therefore, we must have $\tau_\infty = \infty$, *a.s.* This completes the proof. □

3. Study of noise-induced transitions via confidence ellipse

For stochastic model (2.4), when the noise is very small, the random trajectory will leave endemic equilibrium E_* and form a random attractor around it (see Figure 5 (a)-(b)). While for relatively large noise, the dynamic behavior of model (2.4) changed fundamentally. More specifically, the random trajectory can leave the attraction basin of E_*, then cross the boundary (the stable manifold of E_1), and eventually enter the attraction basin of E_0 (see Figure 5(c)-(d)). From a biological perspective, under the random disturbances, the steady state of model (2.4) can switch from the endemic equilibrium to the disease-free equilibrium. In Fig.ure 6, we show random trajectories of model (2.4) with $\sigma = 0.005$ and $\beta_1 = 0.239$ (left), $\beta_2 = 0.237$ (right) respectively. Obviously, with the same noise intensity, the dispersion degree of random trajectory of model (2.4) is significantly different. The reason for this significant difference is that the stochastic sensitivity of endemic equilibrium E_* increases greatly when the parameter β is close to the bifurcation point β^*.

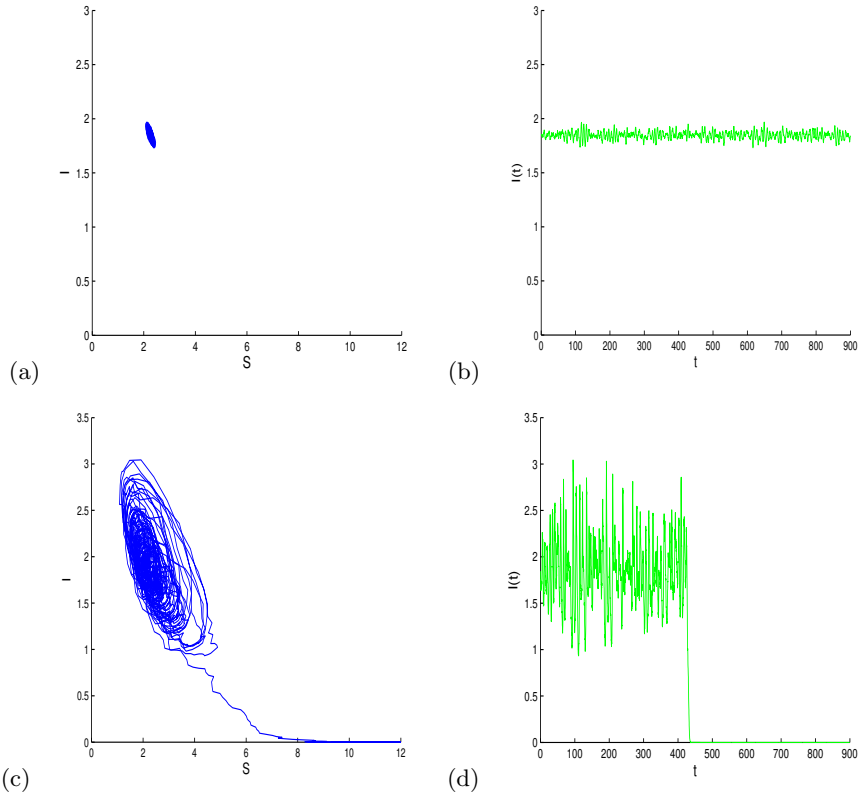

Figure 5. Phase trajectory and time series for stochastic model (2.4) with different noise intensity: (a) and (b) $\sigma = 0.005$, (c) and (d) $\sigma = 0.05$

Next, we use the SSF method [3] to explain the above qualitative analysis in

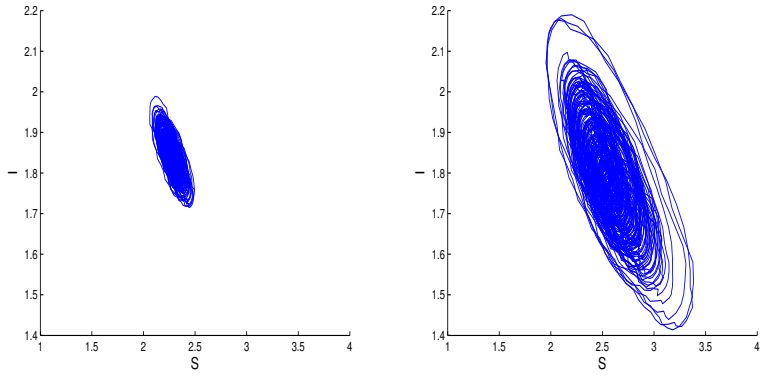

(a) (b)

Figure 6. Random trajectories of model (2.4) with $\sigma = 0.005$ and (a) $\beta_1 = 0.239$, (b) $\beta_2 = 0.237$

details. To this end, denote $E_* = (S_*, I_*)$ and define

$$G = \begin{pmatrix} g_{11} & g_{12} \\ g_{21} & g_{22} \end{pmatrix}, F = \begin{pmatrix} f_{11} & 0 \\ 0 & f_{22} \end{pmatrix}, S = FF^T,$$

where $g_{11} = -\beta I_*^2 - m$, $g_{12} = -2\beta S_* I_*$, $g_{21} = \beta I_*^2, g_{22} = m + \epsilon$ and $f_{11} = S_*$, $f_{22} = I_*$. Solving the system of linear equations as follows:

$$\begin{cases} 2g_{11}w_{11} + g_{12}w_{12} + g_{12}w_{21} = -f_{11}^2, \\ g_{21}w_{11} + (g_{11} + g_{22})w_{12} + g_{12}w_{22} = 0, \\ g_{21}w_{11} + (g_{11} + g_{22})w_{21} + g_{12}w_{22} = 0, \\ g_{21}w_{12} + g_{21}w_{21} + 2g_{22}w_{22} = -f_{22}^2, \end{cases}$$

and we obtain the stochastic sensitivity matrix

$$W = \begin{pmatrix} w_{11} & w_{12} \\ w_{21} & w_{22} \end{pmatrix}.$$

Here, the diagonal elements w_{11} and w_{22} of matrix W represent the sensitivity of endemic equilibrium E_* along S-axis and I-axis. We plot the function curves $w_{11}(\beta)$ and $w_{22}(\beta)$ in Figure 7. As the picture shows, the sensitivity level of the equilibrium point E_* ascends to infinity as the parameter β approaches the bifurcation point β^*. In comparison with Figure 4 and Figure 7, the significant increase in sensitivity is in agreement with the change in the sign of the LLE near the bifurcation point β^*. Indeed, the stability of E_* decreases significantly as the parameter β tends to β^*. This indicates that noise-induced transitions is likely occur. Next, we construct confidence ellipse for E_* by utilizing the SSF method and analyze the phenomenon of stochastic trajectories transitions from E_* to E_0. The confidence ellipse is a

geometrical model which can describe the configurational arrangement of random states near equilibrium E_*. According to [3], the confidence ellipse of E_* is expressed as

$$\left\langle (S-S_*, I-I_*)^T, W^{-1}((S-S_*, I-I_*)^T)\right\rangle = 2\sigma^2 \ln \frac{1}{1-P}, \tag{3.1}$$

where P is a fiducial probability.

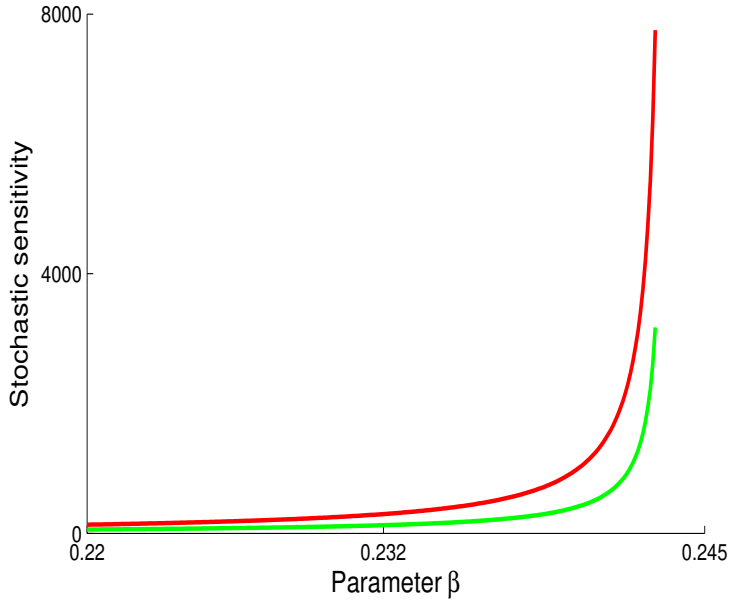

Figure 7. Stochastic sensitivity of equilibrium E_*: w_{11} (red line), w_{22} (green line)

For endemic equilibrium $E_* = (2.26, 1.85)$, in addition to fix parameter $\beta = 0.239$, we take the same parameters as Figure 1, and obtain the stochastic sensitivity matrix and its inverse

$$W = \begin{pmatrix} 1034.94 & -525.05 \\ -525.05 & 427.33 \end{pmatrix}, W^{-1} = \begin{pmatrix} 0.002565 & 0.003152 \\ 0.003152 & 0.006213 \end{pmatrix}.$$

Thus, the confidence ellipse equation of E_* is

$$0.002565(S-2.26)^2+0.006304(S-2.26)(I-1.85)+0.006213(I-1.85)^2 = 2\sigma^2 \ln \frac{1}{1-P}.$$

Throughout the whole article, we take fiducial probability $P = 0.95$. Figure 8 show that the stochastic states of model (2.4) with noise intensity $\sigma = 0.005$ and a corresponding confidence ellipse. In Figure 8, the random states of model (2.4) are distributed around E_*, and their probability of falling inside the confidence ellipse is 0.95. This confidence ellipse can grow and eventually cross the boundary into the attraction basin of disease-free equilibrium E_0 as the noise intensity increases

(see Figure 9). This means that the random trajectory of model (2.4) with high probability escapes from the attraction basin of E_* and being captured by attractor E_0. The noise intensity when the initial intersection of confidence ellipse with the boundary can be considered as a threshold of noise $\tilde{\sigma}$ (here, $\tilde{\sigma} \approx 0.015$). A classic example that the stochastic trajectory leaves the attraction basin of E_* and converges to disease-free equilibrium E_0 is shown in Figure 5(c) where $\sigma = 0.05 > \tilde{\sigma}$.

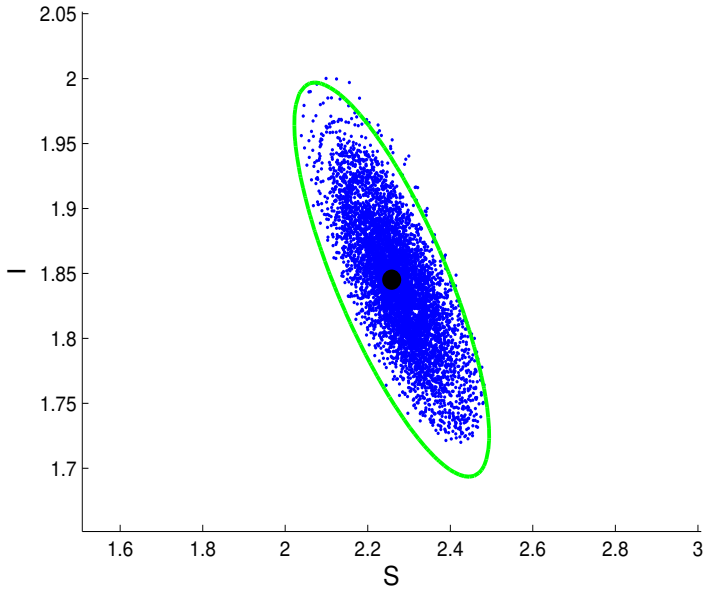

Figure 8. Stochastic states (blue) of model (2.4) and a confidence ellipse (green) for $\sigma = 0.005$

4. Study of noise-induced transitions via confidence band

According to the analysis in the section 2, when the parameter β is in the interval (β_*, β^*), stochastic model (2.4) exists a stable limit cycle Γ around unstable endemic equilibrium E_*. Due to the presence of environmental noise, the random trajectory will leave the deterministic limit cycle Γ and form a stochastic cycle, but the random trajectory will remain in a small neighborhood of Γ for small noise (see Figure 10(a)-(b)). For relatively large noise, the random trajectory will escape from the basin of attraction of Γ and be attracted by attractor E_0 (see Figure 10(c)-(d)). Stochastic cycles of model (2.4) with $\sigma = 0.005$ for $\beta_1 = 0.233$ and $\beta_2 = 0.235$ are shown in Figure 11. It is worth noting that under the influence of the same noise intensity, the distribution of the stochastic cycle around Γ is nonuniform. The above dynamic behavior can be explained by stochastic sensitivity function technique.

Then, we will construct the confidence band for the deterministic limit cycle of

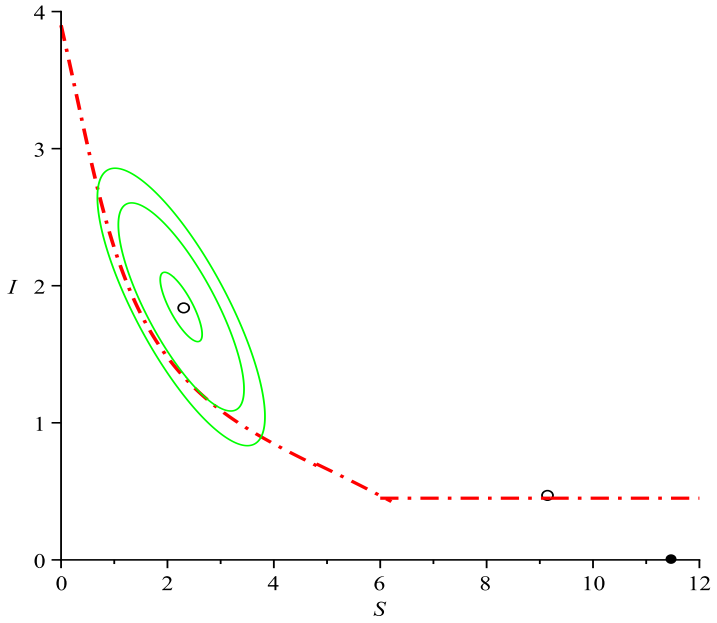

Figure 9. Boundary of attraction basins (red dashed-dotted) and confidence ellipses (green solid) for different noise intensity σ: 0.005 (small), 0.015 (middle), 0.02 (large)

model (2.4) by using SSF technique. To this end, let

$$G_1(S,I) = \Lambda - \beta SI^2 - mS - rS_c,$$
$$G_2(S,I) = \beta SI^2 - mI - \epsilon I,$$

and $\Gamma(S(t), I(t))$, $t \in [0,T]$ represent the limit cycle, where T is the period. We obtain the following matrices:

$$G(t) = \begin{pmatrix} g_{11}(t) & g_{12}(t) \\ g_{21}(t) & g_{22}(t) \end{pmatrix}, F(t) = \begin{pmatrix} f_{11}(t) & 0 \\ 0 & f_{22}(t) \end{pmatrix}, S(t) = F(t)F(t)^T,$$

where

$$g_{11}(t) = (-\beta I^2 - m) \mid_\Gamma, g_{12}(t) = (-2\beta SI) \mid_\Gamma,$$
$$g_{21}(t) = (\beta I^2) \mid_\Gamma, g_{22}(t) = (2\beta SI - m - \epsilon) \mid_\Gamma,$$

and

$$f_{11}(t) = S \mid_\Gamma, f_{22}(t) = I \mid_\Gamma .$$

From [3], $\mu(t)$ satisfies the boundary problem as follows:

$$\begin{cases} \dfrac{d\mu(t)}{dt} = a(t)\mu(t) + b(t), \\ \mu(0) = \mu(T), \end{cases}$$

where

$$a(t) = 2g_{11}(t)p_1^2(t) + 2(g_{12}(t) + g_{21}(t))p_1(t)p_2(t) + 2g_{22}(t)p_2^2(t),$$
$$b(t) = f_{11}(t)p_1^2(t) + f_{22}(t)p_2^2(t).$$

Here,

$$p_1(t) = \frac{G_2(S,I)}{\sqrt{G_1^2(S,I) + G_2^2(S,I)}}\bigg|_\Gamma, \quad p_2(t) = -\frac{G_1(S,I)}{\sqrt{G_1^2(S,I) + G_2^2(S,I)}}\bigg|_\Gamma$$

are elements of a vector function $p(t) = (p_1(t), p_2(t))^T$ orthogonal to vector $(G_1(S,I), G_2(S,I))|_\Gamma$. It follows from [3] that the boundaries $\Gamma_{1,2}(t)$ of the confidence band have the following explicit parametrical form:

$$\Gamma_1(t) = \Gamma(t) + \sigma k\sqrt{2\mu(t)}p(t),$$
$$\Gamma_2(t) = \Gamma(t) - \sigma k\sqrt{2\mu(t)}p(t).$$

where $k = erf^{-1}(P)$. We take different β and plot the function cures $\mu(t,\beta)$ in Figure 12. As seen, the stochastic sensitivity value tends to infinity as the parameter β approaches $\beta_* = 0.233$. This means that the stability of the stochastic cycle will be greatly reduced, so that the noise-induced transitions will occur with high probability. In Figure 13, limit cycle Γ (red line), the bundle of stochastic trajectories (blue line), and confidence band (green dashed) are demonstrated. Obviously, the stochastic trajectories are distributed around Γ, and their probability of falling inside the confidence band is 0.95. The influence of noise intensity on the size of confidence band is shown in Figure 14. As noise intensity increases, the external boundaries of the confidence band will gradually expand and eventually cross the boundary into the attraction basin of disease-free equilibrium E_0.

5. Discussion

Infectious diseases have always been the great enemy of human health. Through out the history, the epidemics of infectious diseases have brought great disasters to human survival and national economy. To study the propagation dynamics and curb strategies of infectious diseases, the mathematical compartmental model is an important method [4]. In this paper, we proposed a stochastic epidemic model and studied noise-induced state shifts from an endemic equilibrium to a disease extinction equilibrium. The corresponding deterministic model can occur bistability (stable equilibria E_*, E_0 or the limit cycle Γ). As the basic transmission rate β changes, we observe the local bifurcations, and the stochastic sensitivity of equilibrium E_* and limit cycle Γ increases sharply when the parameter β approaches β^* and β_*, respectively. The endemic and eradication region are clearly separated by boundary (the stable manifold of E_1). If the initial size of the sub-population is above the boundary, then the disease becomes endemic or the number of infected individuals varies periodically. On the contrary, if the initial size of the sub-population is below the boundary, the disease eventually can be eradicated. However, this boundary can be broken due to the noise fluctuations. The random trajectory may escape from the basins of attraction of attractor (E_* or Γ) and tend to the disease-free equilibrium E_0 (see Figures 5(c) and 10(c)).

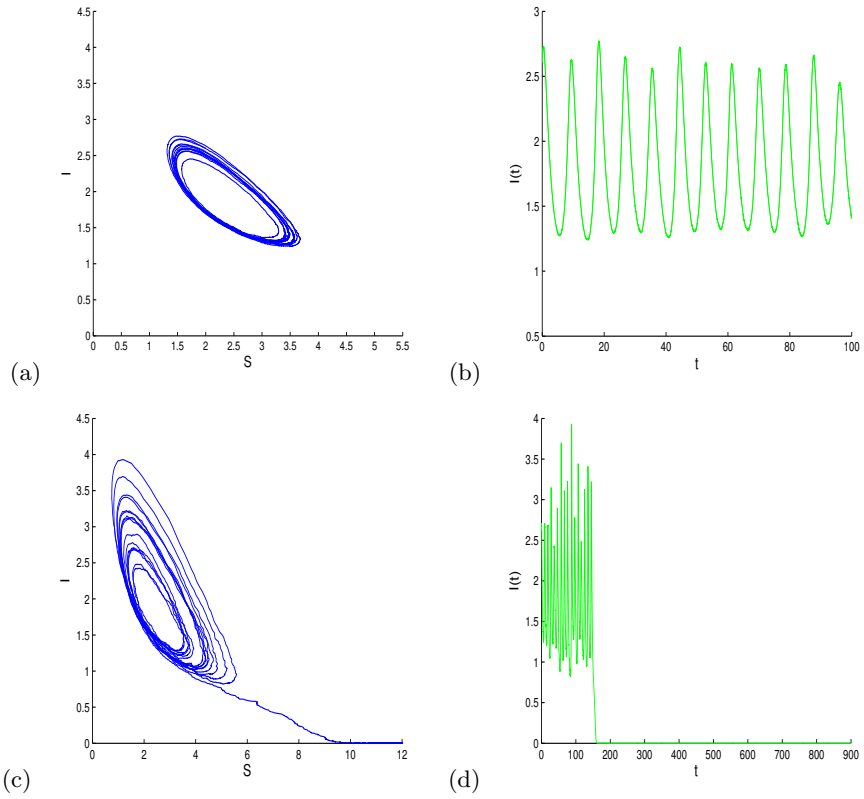

Figure 10. Phase trajectory and time series for stochastic model (2.4) with different noise intensity: (a) and (b) $\sigma = 0.005$, (c) and (d) $\sigma = 0.015$

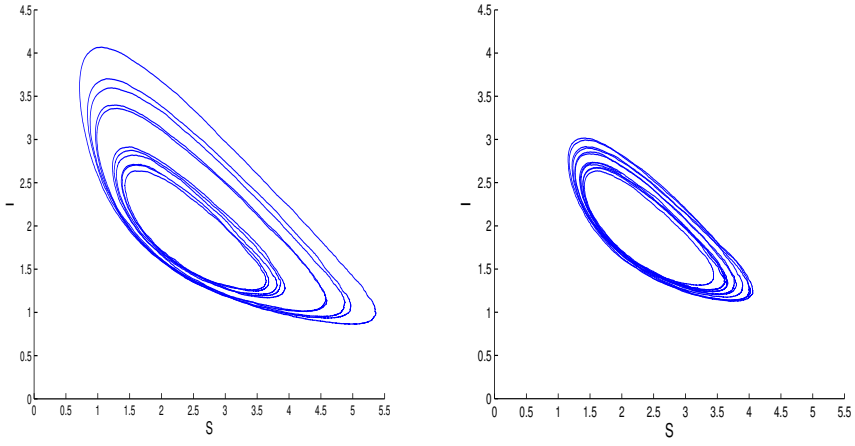

Figure 11. Random trajectories of model (2.4) with $\sigma = 0.005$ and (a) $\beta_1 = 0.233$, (b) $\beta_2 = 0.235$

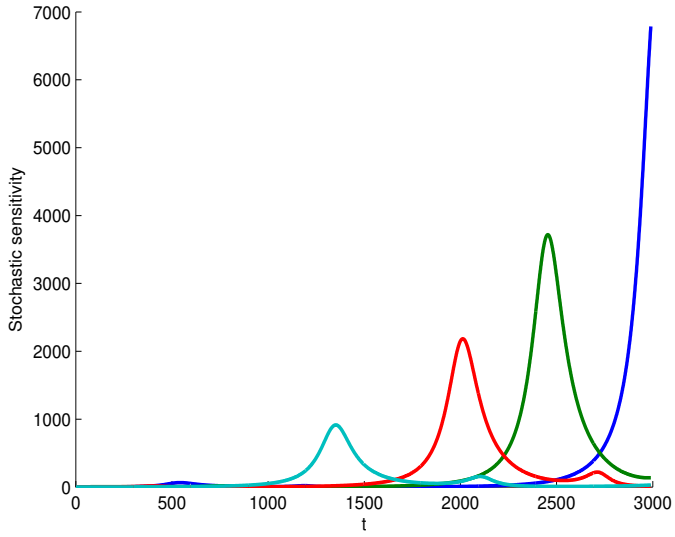

Figure 12. Stochastic sensitivity $\mu(t,\beta)$ of limit cycle Γ for $\beta_1 = 0.235$ (sky blue line), $\beta_2 = 0.234$ (red line), $\beta_3 = 0.2335$ (green line), $\beta_4 = 0.233$ (blue line)

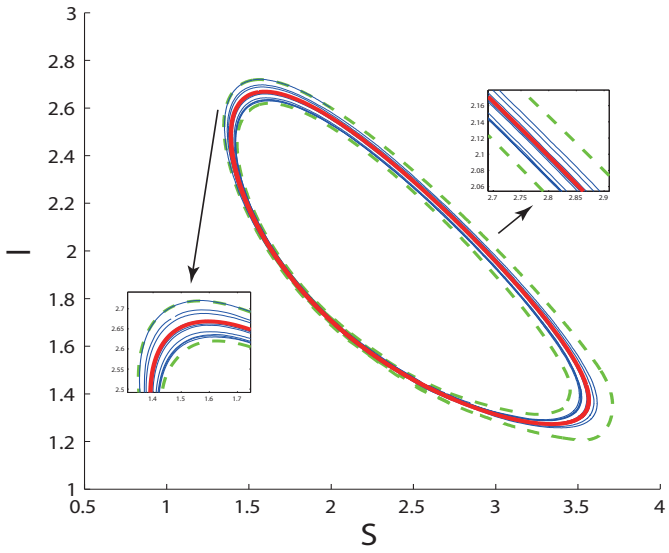

Figure 13. Random trajectories (blue) of stochastic model (2.4) around deterministic limit cycle Γ (red) and confidence band (green) for $\sigma = 0.005$

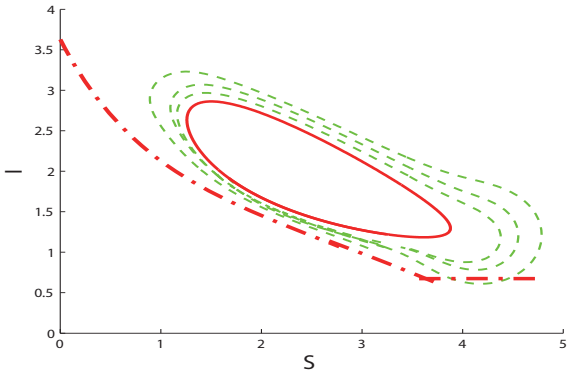

Figure 14. Deterministic cycle for $\beta = 0.235$ and external boundaries (green dashed) of the confidence bands for $\sigma = 0.007$ (small), $\sigma = 0.01$ (middle), $\sigma = 0.015$ (large)

We employ the SSF method to construct confidence ellipse for stochastic model to probe the dynamic behaviors of noise-induced state shifts. For weak noise, the confidence ellipse of E_* near E_* and completely belong to attraction basin of E_* (see Figure 9). However, the confidence ellipse gradually expands and enters into the attraction basin of E_0 as σ increases. The confidence ellipse crossing the boundary means that the stochastic trajectory with a high probability will escape the basin of attraction of E_* and localize near the E_0 (see Figure 5(c)). From a biological perspective, the environmental noise may be benefit to the disease controlling and result in the steady state switching from endemic to disease eradicated. We also constructed the confidence band for limit cycle Γ. The corresponding confidence band assists us to determine the configurational arrangement of stochastic trajectory near the deterministic limit cycle. Then, we study the phenomenon of noise-induced state shifts from a limit cycle to a disease-free equilibrium via confidence band. This paper extends the study of the asymptotic behavior of epidemic models and assists us better understand the dynamics in a random sense. The method in the paper allows to avoid time-consuming direct numerical simulations of the random trajectories in studying noise-induced phenomena. In our future studies, we mainly consider the change of stability of the attraction basin under the disturbance of random factors.

Acknowledgements

The authors express their sincere gratitude to the editors and reviewers for their helpful comments and suggestions.

References

[1] I. Bashkirtseva and L. Ryashko, *Sensitivity analysis of the stochastically and periodically forced Brusselator*, Physica A., 2000, 278, 126–139.

[2] I. Bashkirtseva, L. Ryashko and T. Ryazanova, *Stochastic sensitivity analysis of the variability of dynamics and transition to chaos in the business cycles model*, Communications in Nonlinear Science and Numerical Simulation, 2018, 54, 174–184.

[3] I. Bashkirtseva, T. Ryazanova and L. Ryashko, *Confidence Domains in the Analysis of Noise-induced Transition to Chaos for Goodwin Model of Business Cycles*, International Journal of Bifurcation and Chaos, 2014, 24(8), Article ID 1440020, 10 pages.

[4] B. Boulfoul, A. Kerboua and X. Zhou, *Mathematical Modeling and Analysis of an Epidemic Model with Quarantine, Latent and Media Coverage*, Journal of Nonlinear Modeling and Analysis, 2022, 4(1), 42–63.

[5] Y. Cai, Y. Kang, M. Banerjee and W. Wang, *A stochastic SIRS epidemic model with infectious force under intervention strategies*, Journal of Differential Equations, 2015, 259(12), 7463–7502.

[6] X. Chen, Y. Kang and Y. Fu, *Switches in a genetic regulatory system under multiplicative non-Gaussian noise*, Journal of Theoretical Biology, 2017, 435, 134–144.

[7] Z. Feng, W. Huang and C. Castillo-Chavez, *Global behavior of a multi-group SIS epidemic model with age structure*, Journal of Differential Equations, 2005, 218(2), 292–324.

[8] H. Heesterbeek, R. M. Anderson, V. Andreasen, et al., Modeling infectious disease dynamics in the complex landscape of global health, Science, 2015, 347(6227), aaa4339, 24 pages.

[9] H. W. Hethcote, *The mathematics of infectious diseases*, SIAM Review, 2000, 42(4), 599–653.

[10] G. Lan, S. Yuan and B. Song, *The impact of hospital resources and environmental perturbations to the dynamics of SIRS model*, Journal of Franklin Institute, 2021, 358(4), 2405–2433.

[11] P. Mecenas, R. T. R. M. Bastos, A. C. R. Vallinoto and D. Normando, *Effects of temperature and humidity on the spread of COVID-19: A systematic review*, PLoS ONE, 2020, 15(9), e0238339, 21 pages.

[12] G. N. Mil'Shtein and L. B. Ryashko, *A first approximation of the quasipotential in problems of the stability of systems with random non-degenerate perturbations*, Journal of Applied Mathematics and Mechanics, 1995, 59(1), 47–56.

[13] M. Scheffer and S. R. Carpenter, *Catastrophic regime shifts in ecosystems: linking theory to observation*, Trends in Ecology & Evolution, 2003, 18(12), 648–656.

[14] C. Shan and H. Zhu, Bifurcations and complex dynamics of an SIR model with the impact of the number of hospital beds, Journal of Differential Equations, 2014, 257(5), 1662–1688.

[15] S. Spencer, *Stochastic epidemic models for emerging diseases*, University of Nottingham, 2008.

[16] Y. Sun, Y. Xue and B. Xie, *Dynamics Analysis of an SIS Epidemic Model with the Effects of Awareness*, Journal of Nonlinear Modeling and Analysis, 2021, 3(1), 35–51.

[17] A. Wang, Y. Xiao and R. Smith, *Multiple Equilibria in a Non-smooth Epidemic Model with Medical-Resource Constraints*, Bulletin of Mathematical Biology, 2019, 81, 963–994.

[18] W. Wang, *Backward bifurcation of an epidemic model with treatment*, Mathematical Biosciences, 2006, 201(1–2), 58–71.

[19] W. Wang and S. Ruan, *Bifurcations in an epidemic model with constant removal rate of the infectives*, Journal of Mathematical Analysis and Applications, 2004, 291(2), 775–793.

[20] Y. Xiao and S. Tang, *Dynamics of infection with nonlinear incidence in a simple vaccination model*, Nonlinear Analysis: Real World Applications, 2010, 11(5), 4154–4163.

[21] C. Xu, *Probabilistic mechanisms of the noise-induced oscillatory transitions in a Leslie type predator-prey model*, Chaos, Solitons & Fractals, 2020, 137, Article ID 109871, 11 pages.

[22] A. Yang, B. Song and S. Yuan, *Noise-induced transitions in a non-smooth SIS epidemic model with media alert*, Mathematical Biosciences and Engineering, 2021, 18(1), 745–763.

[23] F. Yang, X. Sun and J. Duan, *On the abrupt change of the maximum likelihood state in a simplified stochastic thermohaline circulation system*, Chaos, 2021, 31(2), Article ID 021103, 6 pages.

[24] S. Yuan, D. Wu, G. Lan and H. Wang, *Noise-induced Transitions in a Non-smooth Producer–Grazer Model with Stoichiometric Constraints*, Bulletin of Mathematical Biology, 2020, 82, 55, 22 pages.

[25] X. Zhang and X. Liu, *Backward bifurcation of an epidemic model with saturated treatment function*, Journal of Mathematical Analysis and Applications, 2008, 348(1), 433–443.

[26] R. Zhao and Q. Liu, *Dynamical Analysis of a Delayed SIQS Epidemic Model on Scale-free Networks*, Journal of Nonlinear Modeling and Analysis, 2021, 3(4), 561–576.